Exosomal miR-29a-3p in the immune microenvironment of spleen deficiency promotes hepatocellular carcinoma lung metastasis by activating FAM167A-α1-integrin-NF-κB signaling axis

Jin Luo
Sun Yat-sen University First Affiliated Hospital
Qiu-Xia Chen
Sun Yat-sen University First Affiliated Hospital
Pan Li
Sun Yat-sen University First Affiliated Hospital
Zhi-Ming Yang
Sun Yat-sen University First Affiliated Hospital
He Yu
Sun Yat-sen University First Affiliated Hospital
Bao-Qi Liu
Sun Yat-sen University Cancer Center
Mei-Ling Fan
Sun Yat-sen University Cancer Center
Zhuo-Mao Mo
Sun Yat-sen University First Affiliated Hospital
Yong-Dan Wang
Sun Yat-sen University First Affiliated Hospital
Mei-Ling Zhou
Sun Yat-sen University First Affiliated Hospital
Hao Hu
Sun Yat-sen University First Affiliated Hospital
Ling Yu
Sun Yat-sen University First Affiliated Hospital
Bi-Jun Huang
Sun Yat-sen University Affiliated Tumor Hospital: Sun Yat-sen University Cancer Center
Shi-jun Zhang (✉ zhshjun@mail.sysu.edu.cn)
Sun Yat-sen University First Affiliated Hospital https://orcid.org/0000-0002-2955-6729

Research Article

Keywords: Exosomes, hepatocellular carcinoma, miR-29a-3p, Spleen deficiency internal environment, Lung metastasis

Posted Date: December 1st, 2022

DOI: https://doi.org/10.21203/rs.3.rs-2266609/v1

Abstract

Background

Hepatocellular carcinoma (HCC), a common type of cancer, has a strong metastatic ability and poor prognosis. The tumor microenvironment is the “soil” for the occurrence and development of tumors, with exosomes playing an important role in these processes. In traditional Chinese medicine(TCM), the tumor microenvironment corresponds to the internal environment of the syndrome known as spleen deficiency (SD). Numerous studies have shown that exosomes contain high levels of miRNAs, which have been shown to contribute to tumor immune regulation and metastasis. The aim of this study was to explore the mechanisms underlying the changes in the tumor microenvironment under the condition of spleen deficiency in order to find better treatments for cancer.

Methods

The effects of exosomal miR-29a-3p on lung metastasis from hepatocellular carcinoma (HCC) were evaluated using the scratch test, migration test, mouse SD model, HCC model, and tail-vein injection model of lung metastasis. The western blot assay, ELISA, flow cytometry, luciferase reporter gene analysis, qRT-PCR and immunofluorescence staining were among the methods used to study the molecular mechanism of lung metastasis promotion under the SD internal environment.

Results

Compared with the mice with HCC only, the mice with HCC and SD symptoms secreted more miR-29a- 3p-enriched exosomes, and their tumor tissue expressed significantly higher levels of α1-integrin and lower levels of FAM167A. These changed the immune microenvironment of mice (Decreased infiltration of T cells ($CD3^+CD4^+$ and $CD3^+CD8^+$), activated α1-integrin-NF-κB signaling pathway, and secreted more interleukin inflammatory factors(IL-1β, IL-6, and IL-8), which promoted the invasion and infiltration of HCC and its lung metastasis both *in vivo* and *in vitro*. In a series of patients with liver cancer, SD was found to have affected their overall survival and relapse-free survival.

Conclusion

Our study showed that under conditions of SD, the body releases more miRNA-containing exosomes, changes the immune microenvironment of the body, and ultimately promotes tumor metastasis and growth. These results highlight potential therapeutic targets and methods for the prevention of cancer metastasis, which may help to screen possible anticachexia TCMs and elucidate its mechanism in the future.

Introduction

Hepatocellular carcinoma (HCC) is the second leading cause of cancer mortality. Metastasis of tumors is one of the most common causes of mortality in HCC. Its etiology and exact molecular mechanisms remain unclear, and therapeutic strategies against it remain unsatisfactory. In patients with HCC, lung metastasis is the most common form of distant disease invasion and progression as well as a leading cause of death[1, 2].Lung metastasis of HCC is affected by many factors, the most important of which is the tumor microenvironment. The liver tumor microenvironment is generally divided into cellular and non-cellular components, including fibroblasts, hepatic stellate cells, immune cells, endothelial cells, mesenchymal stem cells, growth factors, cytokines, extracellular matrix, hormones, and viruses[3].

The “seed–soil” theory holds that the growth[4–6], invasion, and metastasis of tumors are closely related to the tumor microenvironment—“soil”[7], and the overall body environment eventually reaches a level that is conducive to the survival of tumor cells but not of normal cells. When the body environment changes during development, the “big soil” of the internal environment of the organism plays a decisive role in many physiological processes. According to the theory of traditional Chinese medicine (TCM), spleen deficiency (SD) is a core syndrome underlying the pathogenic mechanisms of HCC, with the SD internal environment corresponding to the tumor microenvironment, which as mentioned above provides the “soil” for the occurrence and development of the malignant disease.In clinical practice, we have found that many patients with tumors also have SD symptoms, such as pale complexion, excessive sweating, loss of appetite, abdominal distension, cold body, fatigue, cold hands and feet, and diarrhea[8]. In recent years, therapeutic strategies targeting components of the tumor microenvironment have become a popular choice for combating tumor metastasis[9–12].

Exosomes, which are extracellular vesicles with a diameter of approximately 30–200 nm, are secreted by almost all cells. These vesicles carry a variety of substances, including DNA, RNA, lipids, proteins, and metabolites. Studies have shown that exosomes are involved in various physiological and pathological processes in the human body and play a role in material and information transfer between cells. Exosomal microRNAs (miRNAs) are closely associated with various human diseases[13–16].Specific proteins (e.g., TSG101, CD81, HSP70, CD63, and CD9) that are highly enriched in exosomes are often used to identify the vesicles[17, 18]. Numerous studies have shown that exosomes can mediate communication between cells and tumor-related proteins in the tumor microenvironment and promote tumor metastasis[17–20].

miRNAs are small non-coding RNAs that inhibit the translation of messenger RNAs (mRNAs). It had been shown that exosomes contain high levels of miRNAs, which have been demonstrated to contribute to tumor immune regulation, metastasis, and chemotherapy resistance [21–25]. However, the relationship between plasma-derived exosomal miRNAs extracted from HCC mice with SD and lung metastasis remains unknown.

In this study, we divided mice into two groups: those with HCC with SD symptoms (designated the SD-HCC group) and those with HCC alone (designated the HCC group). A C57 mouse model of SD was also

successfully established and its exosomes were extracted from the plasma. The exosomes extracted from the SD-HCC mice and HCC mice were injected into immunodeficient mice via tail vein injection. In the lung metastasis model, we found that exosomal miRNAs in the SD-HCC mice promoted lung metastasis by secreting more pro-inflammatory cytokines. Our RNA sequencing results suggested that the gene that was differentially expressed between SD-HCC and HCC mice was *FAM167A* (encoding family with sequence similarity 167 member A). Therefore, we speculated that mice with liver cancer and SD could secrete exosomal miR-29a-3p, directly targeting *FAM167A* and changing the immune microenvironment of the body, thereby activating the α1-integrin–nuclear factor-kappa B (NF-κB) signaling pathway and ultimately promoting cancer metastasis. These results highlight potential therapeutic targets for the prevention and treatment of cancer metastasis.

Materials And Methods

Establishment of the mouse model of spleen deficiency and classification criteria for the spleen deficiency index

All animal experiments were approved by the Institutional Animal Care and Use Committee of Sun Yat-sen University, Guangzhou, China. First, 1 mg of reserpine powder (Shanghai McLean Biochemical Technology Co., Ltd., Shanghai, China; CAS code: 50-55-5) was completely dissolved in 25 mL of glacial acetic acid and stored at 4°C as a stock solution. Each mouse was injected subcutaneously with approximately 100 μL of the solution once a day (i.e., 0.1 $mg•kg^{-1}•d^{-1}$) for 14 consecutive days to establish the SD model. The control group was injected subcutaneously with 100 μL of a sodium chloride solution(0.9%) for the same number of days. The body weight and feed amount of all mice were measured daily. Simultaneously, the smell, mental state, body temperature and heat, breathing state, hair color, food intake, and stool of all mice, described in the SD rating scale, were observed and noted.The classification criteria[26–28] for determining the SD index were divided into four grades, each corresponding to a relevant score as follows: a score less than or equal to 7 = no SD symptoms; 8–14 = mild SD; 15–21 = typical SD; and 22–28 = severe SD (Table 1).

Table 1
Classification criteria for determining the spleen deficiency index

Index/Score	Grading standards			
	1	2	3	4
Body odor	Odor-free	Mild odor	Medium odor	Severe odor
Mental state	Stable	Irritable	Fatigued	Somnolent
Fever & chills	Normal	Cowered	Chills	Arched back & trembling
Respiration	Normal	Panting	Tachypnea	Faint
Fur	Glossy	Matted	Fluffy & erect	Brown & erect
Stool	Normal	Wet	Wet & rotten	Mucous texture
Appetite	Normal	Reduced to 50%	Reduced to 25%	None at all

Note: A total score of 7 represents no spleen deficiency, 8–14 represents mild spleen deficiency, 15–21 represents typical spleen deficiency, and 22–28 represents severe spleen deficiency.

Cell lines and culture

Human-derived hepatoma cells (MHCC97H, HCCLM3, and HepG2), mouse-derived hepatoma cells (Hepa1-6), and human embryonic kidney 293T cells were purchased from the American Type Culture Collection (ATCC, Manassas, VA, USA). All cells were cultured in Dulbecco's modified Eagle's medium (DMEM; Gibco, Thermo Fisher Scientific, St. Peters, MO, USA) supplemented with 10% fetal bovine serum (Gibco, Thermo Fisher Scientific) at 37°C in a 5% CO_2 atmosphere.

Extraction of exosomes

The mice were enucleated, and blood was collected in a 1.5 mL anticoagulant tube. The exosomes were then extracted from the plasma using the Wayen Exosome Isolation Kit (Cat# EIQ3-02001, H-Wayen Biotechnologies, Shanghai, China). In brief, 4 μL of reagent C that had been completely thawed on ice was added to 200 μL of mouse plasma, with up and down pipetting and vortex mixing performed until a homogeneous mixture was obtained. Then, 50 μL of extraction reagent A and 50 μL of reagent B were added to the suspension, and exosomes were extracted according to the steps outlined in the manufacturer's instruction manual. Finally, the obtained pellet was resuspended in 50–120 μL of sterilized 1× phosphate-buffered saline (PBS), following which the exosome-containing suspension was aliquoted and stored at − 80°C for further use and analysis.

Transmission electron microscopy

The morphology of the exosomes was examined using a transmission electron microscope (JEM-1200EX, JEOL, Tokyo, Japan). In brief, the purified exosomes were first incubated with 4% osmium tetroxide at 4°C for 30 min, then transferred to copper grids with carbon-coated membranes, and

subsequently stained with 2% phosphotungstic acid for 3 min. The filter paper on which the sample was absorbed was dried for 5 min and then imaged under the electron microscope at 10 kV.

Luciferase reporter gene assay

We predicted the targeting relationship between miR-29a-3p and the *FAM167A* gene using the bioinformatics databases TargetScan (https://www.targetscan.org/vert_80/) and miRDB (http://mirdb.org/). The 3'-untranslated region (3'-UTR) of the *FAM167A* promoter region constituted the miR-29a-3p-binding site for construction of the wild-type (WT) plasmid of *FAM167A* 3'-UTR (FAM167A-WT).

Based on this plasmid, a site mutation kit (Takara, Dalian, China) was used to mutate the miR-29a-3p-binding site on FAM167A-WT to construct the *FAM167A* 3'-UTR mutant (MUT) plasmid (FAM167A-MUT). In the meantime, HCCLM3 cells were seeded into the wells of 24-well plates and grown to 70% confluence. Using Lipofectamine™ 3000 reagent, the correctly sequenced FAM167A-WT or FAM167A-MUT plasmids were then co-transfected into the HCCLM3 cells together with mock NC or mock miR-29a-3p plasmids. At 48 h after transfection, the cells were lysed, and their luciferase activity was detected using a luciferase assay kit (Cat: 11402ES60,Yeasen,Guangzhou, China).

ELISA detection

We used enzyme-linked immunosorbent assay (ELISA) kits (Cat: MM-0163M1, MM-0040M1, and MM-0123M1) to detect target proteins in cell culture supernatants collected in sterile tubes. In brief, after centrifugation of the cell culture at 2–8°C for approximately 20 min (2,000–3,000 rpm), the supernatant was carefully collected and stored. If a precipitate had formed during storage, the supernatant was centrifuged again. The sample was then tested with the ELISA kit according to the manufacturer's instructions. Finally, the optical density at 450 nm of the solution in each well was measured within 15 min of adding the stop solution.

RNA extraction and qRT-PCR

Total RNA was extracted from the cells using the MolPure® Cell/Tissue Total RNA Kit (Cat: 19221ES50, Yeasen, Shanghai, China) and reverse transcribed using SuperScript™ III Reverse Transcriptase (Invitrogen, Thermo Fisher Scientific,Shanghai, China) and specific primers. The real-time reverse transcription-polymerase chain reaction (qRT-PCR) was performed using the SYBR Green PCR Master Mix (Cat: 11184ES08, Yeasen), and detection was performed. The sequences of all the indicated primers are listed in Supplementary Table S1.

Wound-healing and Transwell assay

The mouse HCC cell line Hepa1-6 was co-cultured with approximately 100ug/ml exosomes for 48 h, following which the cells were washed with 2 mL of PBS. Then, 1 mL of 0.25% trypsin was added to dissociate the cells and a pipette was used to disperse them into single cells. Subsequently, 2–3 mL of DMEM containing 10% fetal bovine serum and trypsin was added and the thoroughly mixed cell

suspension was transferred to a 15 mL centrifuge tube. The sample was centrifuged at 1,000 rpm for 5 min, after which the liquid was discarded and 1 mL of the medium was added. After thorough mixing, the cells were counted and 200,000–400,000 were seeded into 2 mL of serum-free DMEM in 6-well plates and cultured at 37°C. After overnight incubation, the medium was removed, and the cell layer in each well of the 6-well plate was scratched with a 200 μL pipette tip. The cells were then washed with PBS, and 1 mL of the wash solution was used for imaging analysis (adding PBS before photography to avoid a medium-colored background). After scratching of the cell layer, a time gradient was used, where images were taken at 12, 24, and 48 h.

For the cell migration assay, 800 μL of DMEM containing 10% fetal bovine serum was added to the lower chambers of a 24-well Transwell plate, and 200 μL of a serum-free cell suspension was added to the cell culture inserts in the upper chambers. The cells were cultured in an incubator for 20–24 h (no more than 24 h to avoid cell proliferation affecting the migration experiment). Then, the cell culture inserts were carefully removed from the chambers with tweezers, and the upper chambers and lower chambers were blotted to remove liquids and then washed with PBS. The cell culture inserts were then returned to the wells and 800 μL of methanol was added to the lower chamber and 200 μL to the upper chamber. After the cells had been fixed at ambient temperature (25℃) for 15 min, the methanol was removed from the chambers. The upper and lower chambers were again blotted and the fixatives were dried, after which 800 μL of crystal violet was added to the lower chamber and 200 μL to the upper chamber. The cell culture inserts were incubated for 30 min at ambient temperature, following which they were gently rinsed, then soaked several times with water, and finally removed from the chamber and blotted dry. The upper chamber liquid was blotted, and the cells were carefully wiped from the membrane surface on the bottom of the upper chamber with a damp cotton swab. The plates were inverted and dried thoroughly overnight in the oven. Pictures were taken, and samples were obtained.

Nude mouse tumor xenograft models

To generate tumor xenograft models, 0.1 mL of a precultured Hepa1-6 cell suspension (1×10^7/mL) was injected subcutaneously into the armpit of BALB/C nude mice. When the subcutaneous tumors were approximately 1 cm in diameter (after ~ 2 weeks), the mice were anesthetized with a 1% sodium pentobarbital solution (50 mg/kg) and then euthanized by cervical dislocation. The tumor was rapidly excised under sterile conditions, and the meat-like tissue was cut into 1 mm^3 small pieces in PBS solution. The mouse model of liver cancer was then established as follows. First, the skin of C57 mice was incised at the xiphoid process under anesthesia, and the left liver lobe was removed from the abdominal cavity. A 1 mm^3 piece of the tumor tissue was placed in a cannula (5 mm from the tip), which was then inserted into the liver surface at a 10° angle. Then, the tumor tissue was implanted under the liver capsule, an absorbable gelatin sponge was applied to the bleeding area, and the liver lobes were returned to the abdominal cavity, which was subsequently flushed with penicillin solution and closed with absorbable sutures. Blood and tissue samples were collected 28 d after the establishment of the liver cancer model.

Western blot analysis

The liver cancer tissues and HCC cells of the two groups of mice were lysed using RIPA lysis buffer, following which the total proteins were extracted using the corresponding extraction kit. The manufacturer instructions, “gel preparation–electrophoresis–transfer membrane–blocking and incubation antibody–incubate secondary antibody–ECL luminescence,” were then followed step by step, and finally data statistics and images were obtained. Primary antibodies used in this study were FAM167 Ab (1:1000),α1-integrin Ab (1:1000), Alix Ab (1:1000), HSP70 Ab (1:1000), CD81 Ab (1:1000), NF-κB Ab (1:1000), phosphorylated-NF-κB Ab (1:1000), and GAPDH mAb (1:1000). Secondary antibodies were anti-rabbit (1:2000) and anti-mouse (1:2000).

Survival analysis

The Kaplan–Meier plotter (http://kmplot.com/), which is an interactive online tool for investigating survival correlations, can assess the effects of 54,000 genes on survival in 21 cancer types [29]. To determine the clinical significance of the α1-integrin and *FAM167A* genes, patients with HCC were divided into high- and low-expression groups. The overall survival (OS) and recurrence/relapse-free survival (RFS) rates of the two groups were assessed using Kaplan–Meier plots and the log-rank *p*-value ($p < 0.05$). The past 10 years of follow-up statistics of 70 liver cancer patients of the Department of Traditional Chinese Medicine of the First Affiliated Hospital of Sun Yat-sen University were used for the OS and RFS analyses with the R language.

RNA interference and plasmids

Small interfering RNAs (siRNAs) (viz., siNC and siRNAs targeting *FAM167A* or α1-integrin) and mimics of the indicated miRNAs were obtained from Kinco Co., Ltd. (Beijing, China). The sequences of the siRNAs and miRNA mimics are listed in Supplementary Table S2. Lentiviral vectors containing the miR-29a-3p inhibitor and control sequence were constructed and generated by GeneCopoeia (Rockville, MD, USA). The selection of lentiviral-transfected cells using puromycin was performed by Guangzhou Weijia Technology Co., Ltd. (Guangzhou, China).

Immunohistochemistry and immunofluorescence staining

The 2-Step Plus Poly-HRP Anti Mouse/Rabbit IgG Detection System (with DAB solution) (E-IR-R217-6 mL, Elabscience, Wuhan, China) and immunofluorescence staining kit (Cat: E-IR-R323-100T, Elabscience) were used for detecting target proteins by immunohistochemistry and immunofluorescence staining, respectively. First, the mouse liver cancer tissue was fixed with 4% cold paraformaldehyde for 15 min and then washed three times with PBS. This was followed by membrane perforation, blocking, primary antibody incubation, and secondary antibody incubation steps, and finally 0.5 μg/mL 4',6-diamidino-2-phenylindole was added for nuclear staining. Immunohistochemistry was performed using semi-quantitative methods, and the percentage of positive cells and staining intensity were scored under a microscope.

Establishment of the lung metastasis model via tail vein injection

Twenty immunodeficiency mice were randomly divided into HCC and SD-HCC groups. Then, the HCC group was injected with MHCC97H-luc liver cancer cells and exosomes extracted from the plasma of mice with liver cancer only, whereas the SD-HCC group was injected with MHCC97H-luc liver cancer cells and exosomes extracted from the plasma of mice with liver cancer and SD symptoms. The exosomes were mixed and injected into the immunodeficiency mice via the tail vein. The number of cells was 10^6/100 μL per mouse, and the exosome dose was 10 μg•mouse^{-1}•week^{-1}. After 6 weeks, each mouse was administered an intraperitoneal injection of 150 mg/kg fluorescein sodium salt (Cat. No: 4090ES03, Yeasen). After subjecting the nude mice to gas anesthesia, tumor growth in each mouse was detected using the AniView100 multimodal animal *in vivo* imaging system. Thereafter, the nude mice were euthanized, and lung tissue was harvested for hematoxylin and eosin (HE) staining.

Hematoxylin and eosin staining

Tissue sections were dewaxed with xylene for 10 min and then rehydrated using an ethanol gradient (100%, 95%, 80%, 70%, and 60%) for 5 min at each concentration. Thereafter, the sections were stained with hematoxylin for 2 min, differentiated in ethanolic hydrochloric acid for 20 s, stained with eosin for 10 min, and then rinsed with tap water. Finally, the sections were sealed with neutral resin and examined under a microscope.

Flow cytometry

The spleens of the two groups of mice were removed, stored in RPMI-1640 medium, and immediately crushed within 4 h to prepare single-cell suspensions. The immune cells were subsequently detected through staining with antibodies against the following mouse antigens: anti-CD3, anti-CD45, anti-CD4, and anti-CD8. CD45 MicroBeads (Miltenyi, Bergisch Gladbach, Germany) were used to enrich the tumor-infiltrating immune cells, which were then analyzed using FlowJo v10.0 or FACS Diva v8.0 software, according to the manufacturer's instructions. The difference in immune cell proportions between the two groups of mice was calculated.

Statistical analysis

GraphPad Prism software (GraphPad Software, La Jolla, CA, USA) was used to perform all statistical analyses. Each experiment was conducted in at least triplicates, with all results presented as the mean ± standard deviation. The χ^2 and Student's *t*-test were used to assess the statistical significance of differences between the various mouse groups. Analysis of variance with Tukey's multiple comparisons post-hoc test and Pearson's correlation analysis were performed for statistical comparisons. Kaplan–Meier analysis and log-rank tests were applied for the survival analyses. A *p*-value of less than 0.05 was considered statistically significant.

Results

Spleen deficiency changed the body weight, appetite, Mental state and other indicators in mice

Two groups of normal male specific-pathogen-free C57BL/6 mice were used: one group was injected with reserpine (0.1 mL/10 g, once a day for 14 d), and the other group was injected with an equal volume of normal saline. One week later, the pre-prepared HCC tumor from a nude mouse was cut into 1 mm^3 pieces and orthotopically transplanted into the livers of the above two groups of mice, thereby generating mice with HCC only (HCC group) and those with both SD and HCC (SD-HCC group).

We analyzed the body weight and daily feed amount of the C57BL/6 mice before, during, and after SD modeling and found that there was no statistical difference between the two groups before modeling ($p > 0.05$) (Fig. 1a, d). However, statistically significant differences were found between the two groups during and after the SD modeling process ($p < 0.001$) (Fig. 1b, c, e, f). At the same time, the SD scores between the two groups were significantly different before and after modeling ($p < 0.001$) (Fig. 1g).

Spleen deficiency promoted the secretion of more exosomes in mouse plasma, thereby promoting cell migration, invasion, and wound healing in vitro

There is an abundance of evidence that tumor metastasis is closely related to the tumor microenvironment[30–32].In this study, exosomes were extracted from mouse plasma using an exosome isolation kit, and their cup-shaped structure, size, and number were determined using electron microscopy and Nanosight particle tracking analysis (Fig. 2a, b). We found that the C57 mice that had been injected with reserpine for 14 d secreted more exosomes after successful SD modeling than the normal C57 mice did (Fig. 2b, c). The exosome markers were all detected on the western blot, where their protein contents were significantly higher than those of the control group (Fig. 2d). Next, we added exosomes extracted from the plasma of mice with SD to the liver cancer cell lines MHCC97H and Hepa1-6 for co-culture and tested their migratory activity using the Transwell assay. Surprisingly, the liver cancer cells in the exosome-treated group had stronger migration and invasion abilities than those in the blank control group. Moreover, the cancer cells treated with exosomes from the mice with SD had stronger migration and invasion abilities than the cells treated with exosomes from a normal mice (Fig. 2e, f, g, h). Additionally, we added the plasma-derived exosomes from the SD-HCC and HCC groups of mice to Hepa1-6 cells to conduct scratch experiments and found that the extracellular vesicles from mice with SD symptoms could better promote cell wound healing (Fig. 2i, j).

MiR-29a-3p released by exosomes from mice with spleen deficiency affected FAM167A–α1-integrin activation of the NF-κB pathway and the promotion of inflammatory cytokine release

We sent the two groups of exosomes for sequencing and obtained 15 miRNAs with statistically significant differences between the groups, among which the up-regulation of miR-29a-3p was the most obvious (Fig. 3a). Then, we performed qRT-PCR analysis of the two groups of exosomes to obtain the multiple differences in miR-29a-3p between them on the RNA level (Fig. 3b). We performed RNA sequencing analysis of the liver cancer tissues from the HCC and SD-HCC groups of C57 mice. The conditions for screening differentially expressed gene sequences were a fold change value of greater than 1 and a *p*-value of less than 0.05. As a result, the genes coding for FAM167A, α1-integrin, and

serglycin were found to differ significantly between the two mouse groups (Fig. 3c). (Serglycin has been studied in depth in another article and is not discussed herein.) A heatmap of the sequences was generated using TBtools software[33].Using miRDB and TargetScan, the target gene of miR-29a-3p was predicted to be *FAM167A* (Fig. 3d). Alignment of the miR-29a-3p sequence with the full-length *FAM167A* sequence confirmed that the *FAM167A* coding sequence was a potential target of this miRNA (Fig. 3e). Subsequently, we cloned the binding sites of WT and MUT miR-29a-3p into the luciferase vector for transfection into HCCLM3 cells. The luciferase assay results showed that in HCCLM3 cells, the vector containing the WT binding site caused a significant decrease in luciferase activity, whereas cells transfected with the MUT binding site did not show this trend (Fig. 3f). Additionally, we transfected cells with the mimics and siRNAs of miR-29a-3p and α1-integrin for 48 h and then extracted the cellular proteins for analysis. The western blot results showed that the miR-29a-3p mimic or knockdown of *FAM167A* promoted the expression of α1-integrin, and miR-29a-3p high expression or *FAM167A* inhibition also promoted NF-κB phosphorylation (Fig. 3g). More importantly, knockdown of α1-integrin attenuated the effect of miR-29a-3p on NF-κB phosphorylation (Fig. 3h). To further investigate the effect of miR-29a-3p, HCC cells were stably transfected with an miR-29-3p inhibitor. As a result, the impact of miR-29a-3p on the cells was abolished by its specific inhibitor (Fig. 3i, j). Additionally, we found that the miR-29a-3p mimic also contributed to the motility of HCC cells (Fig. 3k, l). It is well known that interleukin (IL)-1β, IL-6, and IL-8 are targets of NF-κB. We found that the mRNA levels of IL-1β, IL-6, and IL-8 in cells co-cultured with exosomes from the mice with SD were higher than the levels in cells co-cultured with exosomes from mice without SD and in the blank control group (Fig. 3m). The ELISA results confirmed that the levels of the IL-type factors in the supernatant of the cells were increased to varying degrees (Fig. 3n). Collectively, these results suggest that exosomal miR-29a-3p from SD-HCC mice mediates α1-integrin and *FAM167A* gene expression and activates the NF-κB pathway. Specifically, it promotes NF-κB phosphorylation and increases the levels of the IL-type factors, thereby promoting cancer cell migration and invasion.

Spleen deficiency changed the tumor immune microenvironment and promoted tumor growth in vivo

To further explore how the internal environment of the body changes under SD conditions, we generated Hepa1-6 tumors in the armpits of BALB/C mice and then transplanted the tumor tissue into the liver of spleen-deficient C57 mice. We found that the tumor size in mice with SD was significantly larger than that in the mice without the syndrome (Fig. 4a, b). We then used qRT-PCR to detect the α1-integrin expression level in the liver cancer tissues of the two groups of mice and found that the level was significantly higher in the SD-HCC group (Fig. 4c). The same trend was obtained in the western blot analysis of this protein (Fig. 4D). Immunohistochemical analysis of tissue sections of the tumors also verified that the α1-integrin expression level was higher in the SD-HCC group(The positive rate of tumor cells was higher in the SD-HCC group) (Fig. 4e, f). We used immunofluorescence staining to detect the difference in FAM167A levels between the two groups and found that it was lower in the SD-HCC group (Fig. 4g), which was opposite to the α1-integrin expression level (Fig. 4h). HE staining of the two groups of tissues showed that the SD-HCC group had a higher cell density, a disordered arrangement, more multinucleated cells, destruction of the hepatic cord and sinusoids, and a higher degree of liver stasis and cirrhosis (Fig. 4i).

Secreted exosomes in SD-HCC mice accelerated the lung metastasis process

According to previous studies, exosomes and integrins are closely associated with cancer metastasis[34–37]. In our study, mouse exosomes and integrins showed apparent changes under the SD internal environment. Therefore, to further clarify whether these changes were related to tumor metastasis, we established a lung metastasis model in immunodeficient mice. To this end, the HCC group was injected with MHCC97H-luc liver cancer cells and plasma-derived exosomes from mice with liver cancer only, whereas the SD-HCC group was injected with MHCC97H-luc liver cancer cells and plasma-derived exosomes from mice with liver cancer and SD. The exosomes were respectively mixed with the hepatoma cells and injected into immunodeficiency mice via the tail vein. After 6 weeks, fluorescein sodium salt was administered intraperitoneally into each mouse for in vivo imaging of the animals (Fig. 5a). The metastatic lung nodules in the SD-HCC group had enhanced fluorescein intensity and were larger in area. We euthanized the mice and stained the lung tissue with HE (Fig. 5c). Surprisingly, the SD-HCC group not only had an increased amount of lung metastases (Fig. 5e) but also a higher degree of tissue differentiation and a higher cell density. The increased disorderly arrangement occurred mostly with the multinucleated cells. Immunohistochemical analysis of the differences in FAM167A, α1-integrin, and p-NF-κB gene expression between the two groups of tissues revealed consistency of their levels with the previous *in vitro* results, in that the α1-integrin and p-NF-κB levels were increased and the FAM167A level was decreased in SD-HCC lung metastasis (Fig. 5f). We selected cases from the Gene Expression Omnibus and The Cancer Genome Atlas databases and analyzed the OS and RFS rates in relation to the *FAM167A* and α1-integrin genes. The results, which were calculated from the time the disease was first diagnosed, also revealed that low FAM167A and high α1-integrin expression levels were associated with shorter OS and RFS in liver cancer. (Fig. 5b, d).

Spleen deficiency changed the immune state of mice and affected the overall survival and relapse-free survival of patients with liver cancer

In order to further explore the specific mechanism of action, we did a further experiment and follow-up of patients with liver cancer. We did flow cytometry to analyze the changes in the relevant immune cells. Flow cytometric analysis of the level of spleen cell infiltration in the two groups of mice showed decreased infiltration of T cells ($CD3^+CD4^+$ and $CD3^+CD8^+$) in the SD-HCC group (Fig. 6a, b, c).We had followed up on 70 liver cancer patients at the Department of Traditional Chinese Medicine of the First Affiliated Hospital of Sun Yat-sen University in the past 10 years.We found that the patients without symptoms of SD (LC group) had significantly longer OS (Fig. 6d) and RFS rates (Fig. 6e) than the patients with symptoms of SD (SD-LC group).

Discussion

The tumor microenvironment, a dynamic system coordinated by intercellular communication, is closely related to tumor progression and metastasis [38–43].Clinically, we have found that patients with SD symptoms are more likely to develop cancer, and cancer patients with SD symptoms have higher rates of

metastasis and mortality and a shorter tumor-free survival time after surgery than those without such symptoms. The malignant disease progresses rapidly in patients with SD.

Because there is a paucity of data on the effects of an SD internal environment on HCC metastasis, we constructed animal models of SD-HCC and of orthotopically transplanted liver cancer (HCC), extracted plasma exosomes from the two groups of mice, and injected them into immunodeficient mice through the tail vein to observe the effects of lung metastasis. We found that the SD-HCC mouse-derived exosomes had a significantly enhanced ability in promoting lung metastasis compared with the HCC mouse-derived exosomes. We performed cell experiments with the extracted exosomes and also found that the SD-HCC group could better promote the migration and invasion abilities of liver cancer cells. RNA sequencing analysis of the liver cancer tissues revealed apparent differences between the two mouse groups. Finally, miRDB and TargetScan predicted *FAM167A* as the target gene of miR-29a-3p. FAM167A is found in some leukemias and lymphomas and is typically associated with a poor prognosis [44].

Subsequently, we added the mimic and siRNA of miR-29a-3p and α1-integrin to cancer cell cultures and extracted cellular proteins 48 h after transfection. Western blot analysis showed that knockdown of the miR-29a-3p mimic or *FAM167A* promoted the expression of α1-integrin, and miR-29a-3p expression or FAM167A inhibition also promoted NF-κB phosphorylation. More importantly, knockdown of α1-integrin attenuated the effect of miR-29a-3p on NF-κB phosphorylation. Integrins are cell surface receptors composed of α and β subunits. Studies have shown that integrins accelerate cell migration by promoting the nuclear transport of NF-κB and activating the NF-κB signaling pathway, which is closely related to tumor metastasis [45]. To further investigate the effects of miR-29a-3p, HCC cells were stably transfected with an miR-29-3p inhibitor, which abolished the effects of the miRNA on cells, as expected. Additionally, we found that the mRNA levels of IL-1β, IL-6, and IL-8 in cells exposed to SD-HCC mouse-derived exosomes for 72 h were higher than the levels in cells exposed to HCC mouse-derived exosomes and cells in the blank control group. These findings reveal that exosomal miR-29a-3p in the SD-HCC environment regulates the gene expression of α1-integrin and *FAM167A*, activates the NF-κB pathway, promotes phosphorylation, and increases inflammatory IL-type factor levels, thereby ultimately promoting cancer cell migration and invasion and eventually leading to lung metastasis (Fig. 6f).

First invoked by Paget, the seed and soil hypothesis suggests that the successful growth of metastatic cells depends on the interactions and properties of cancer cells (seeds) and their potential target organs (soil). The “seed–soil” theory holds that cancer cells (seeds) must find their appropriate soil to growth, invasion, and metastasis. The “soil”, the body’s internal environment, which is also called as the body with SD syndrome in TCM theory. It is the core pathogenic mechanism for the occurrence and development of malignant disease.

In previous studies, there have been many discussions about exosomes promoting tumor growth and metastasis [46–48]. Metastatic organogenesis has been one of the greatest mysteries since Stephen Paget’s 1889 “seed–soil” hypothesis was introduced. Exosomal proteomics has revealed distinct integrin

expression patterns, and numerous studies have demonstrated that exosomal integrins can be used to predict organ-specific cancer metastasis [49, 50].

There are new exciting strategies in the fight against cancer, with changing the tumor microenvironment and implementing immunotherapy methods being breakthroughs in cancer treatment development [51, 52]. Many studies have shown that the human body is in a state of immunodeficiency when SD symptoms are present [53–55]. Therefore, it is of great significance to improve the symptoms of SD and change the human body environment for improving immunity. We also found that exosomal miR-29a-3p in the SD internal environment promotes the metastasis of HCC via activation of the FAM167A–α1-integrin–NF-κB signaling pathway. It has been reported [44], that the *FAM167A* gene can activate the NF-κB pathway and induce BCR–ABL-independent tyrosine kinase inhibitor resistance. The FAM167A protein activates the non-canonical NF-κB pathway by binding to desmoglein-1 (DSG1), a cell adhesion protein. Under the state of SD, exosomes can activate the NF-κB signaling pathway in liver cancer cells and significantly promote the expression of phosphorylated NF-κB. Studies have shown that exosomes and integrins are closely related to tumor metastasis [56–58],Our study showed that the levels of exosomes and integrins will increase significantly under the state of SD, leading to activation of the NF-κB pathway and the promotion of NF-κB phosphorylation, which also changes the tumor immune microenvironment and reduces the proportion of $CD4^+$ and $CD8^+$ immune cells.

These findings have important guiding significance for our clinical practice. For patients with TCM symptoms of SD, we can apply Chinese herbs for strengthening the spleen and replenishing the “qi” for symptomatic treatment, starting on the basis of the “seed–soil” theory to change the microenvironment that tumors rely on for survival. Our follow-up project will be to study the therapeutic mechanisms of related TCMs. Such as Spleen strengthening medicine ingredient atractylodes enol, quercetin, etc. One particularly exciting candidate is quercetin, an active ingredient in the Chinese medicinal plants *Lobelia* and *Scutellaria barbata*. It is hoped that more effective ingredients for both SD and cancer treatment can be found in natural medicines to overcome the global problem of malignant diseases in humans.

Conclusions

In conclusion, our study showed that under conditions of SD, the body releases more miRNA-containing exosomes, which mediate the gene expression of α1-integrin and *FAM167A*, activate the NF-κB pathway, and promote the release of more IL-type inflammatory factors. At the same time, SD changes the immune microenvironment of the body and ultimately promotes tumor metastasis and growth. TCM strategies for strengthening the spleen and its active components can start from the “seed–soil” theory; that is, to change the immune microenvironment or “soil” wherein tumors survive. The mechanism of such therapeutic strategy needs to be further studied and explored before it can be applied clinically.

Abbreviations

ATCC: American Type Culture Collection

DMEM: Dulbecco’s modified Eagle’s medium

ELISA, enzyme-linked immunosorbent assay

HCC: Hepatocellular carcinoma

HE: hematoxylin and eosin

LC: liver cancer

miRNA: microRNA

mRNA: messenger RNA

MUT: mutant

OS: overall survival

PBS: phosphate-buffered saline

qRT-PCR: real-time reverse transcription-polymerase chain reaction

RFS: recurrence/relapse-free survival

RIPA: Radio Immunoprecipitation Assay

SD: spleen deficiency

SD-HCC: Hepatocellular carcinoma in spleen deficiency syndrome

siRNAs: small interfering RNAs

TCM: traditional Chinese medicine

UTR: untranslated region

WT: wild type

Declarations

Ethics approval and consent to participate

All animals received humane care throughout the experiments. The study protocols were approved by the Committee on the Use of Clinical Research and Animal Trials of the First Affiliated Hospital of Sun Yat-sen University (Number: Ethical review [2020] No.402).

Consent for publication

Not applicable.

Availability of data and materials

The datasets used and/or analyzed during the present study are available from the corresponding author upon reasonable request.

Competing interests

The authors declare that they have no competing interests.

Funding

This study was supported by the National Natural Science Foundation of China (No. 81873248, 82174173, 81903967, 82104962, 82104647, 81972785, and 81773162) and the Postdoctoral Science Foundation of China (No. 2021M700964). The study was also supported by the Project of Inheriting Famous TCM Masters of Guangdong Provincial Administration of Traditional Chinese Medicine (No. [2020]1), China (No. 2017A030313866 and 2022A1515012298 to B.H.) and the Open Funds of State Key Laboratory of Oncology in South China (No. HN2021-09).

Author contributions

JL, QC, and PL designed the experiments, analyzed the data, and prepared the manuscript. SZ, BH, HH, LY, and CQ conducted the experiments. ZM, BL, ZM, YW, MZ, ML, and HY devised the methodology, collected data, and provided the specimens. All authors confirmed the final manuscript.

Acknowledgements

Not applicable.

References

1. N.N. Pavlova, J. Zhu, C.B. Thompson, The hallmarks of cancer metabolism: still emerging, Cell Metab 34(3) (2022) 355-377.
2. K. Uka, H. Aikata, S. Takaki, H. Shirakawa, S.C. Jeong, K. Yamashina, A. Hiramatsu, H. Kodama, S. Takahashi, K. Chayama, Clinical features and prognosis of patients with extrahepatic metastases from hepatocellular carcinoma, World J Gastroenterol 13(3) (2007) 414-420.
3. H. Wang, L. Chen, Tumor microenviroment and hepatocellular carcinoma metastasis, J Gastroenterol Hepatol 28 Suppl 1 (2013) 43-48.
4. Y.T. Liu, S. Goel, M. Kai, G.J. Moran, T. Nguyen, J. Mai, H. Shen, A. Ziemys, K. Yokoi, Seed- and soil-dependent differences in murine breast tumor microenvironments dictate anti-pd-l1 igg delivery and therapeutic efficacy, Pharmaceutics 13(4) (2021).

5. M. Akhtar, A. Haider, S. Rashid, A. Al-Nabet, Paget's "seed and soil" theory of cancer metastasis: an idea whose time has come, Adv Anat Pathol 26(1) (2019) 69-74.
6. K. Vandyke, Seed and soil revisited in multiple myeloma, Blood 137(17) (2021) 2282-2283.
7. J. Mikula-Pietrasik, P. Uruski, A. Tykarski, K. Ksiazek, The peritoneal "soil" for a cancerous "seed": a comprehensive review of the pathogenesis of intraperitoneal cancer metastases, Cell Mol Life Sci 75(3) (2018) 509-525.
8. L. Sun, J.J. Mao, Y. Yan, Y. Xu, Y. Yang, Patient reported traditional chinese medicine spleen deficiency syndrome (tcm-sds) scale for colorectal cancer: development and validation in china, Integr Cancer Ther 20 (2021) 1543335241.
9. L. Bejarano, M. Jordao, J.A. Joyce, Therapeutic targeting of the tumor microenvironment, Cancer Discov 11(4) (2021) 933-959.
10. J.E. Bader, K. Voss, J.C. Rathmell, Targeting metabolism to improve the tumor microenvironment for cancer immunotherapy, Mol Cell 78(6) (2020) 1019-1033.
11. N.M. Anderson, M.C. Simon, The tumor microenvironment, Curr Biol 30(16) (2020) R921-R925.
12. D.C. Hinshaw, L.A. Shevde, The tumor microenvironment innately modulates cancer progression, Cancer Res 79(18) (2019) 4557-4566.
13. Y. Li, Z. Yin, J. Fan, S. Zhang, W. Yang, The roles of exosomal mirnas and lncrnas in lung diseases, Signal Transduct Target Ther 4 (2019) 47.
14. Z. Sun, K. Shi, S. Yang, J. Liu, Q. Zhou, G. Wang, J. Song, Z. Li, Z. Zhang, W. Yuan, Effect of exosomal mirna on cancer biology and clinical applications, Mol Cancer 17(1) (2018) 147.
15. F. Yang, Z. Ning, L. Ma, W. Liu, C. Shao, Y. Shu, H. Shen, Exosomal mirnas and mirna dysregulation in cancer-associated fibroblasts, Mol Cancer 16(1) (2017) 148.
16. J. Zhang, S. Li, L. Li, M. Li, C. Guo, J. Yao, S. Mi, Exosome and exosomal microrna: trafficking, sorting, and function, Genomics Proteomics Bioinformatics 13(1) (2015) 17-24.
17. A. Bobrie, C. Thery, Exosomes and communication between tumours and the immune system: are all exosomes equal? Biochem Soc Trans 41(1) (2013) 263-267.
18. A. Bobrie, M. Colombo, S. Krumeich, G. Raposo, C. Thery, Diverse subpopulations of vesicles secreted by different intracellular mechanisms are present in exosome preparations obtained by differential ultracentrifugation, J Extracell Vesicles 1 (2012).
19. V. Luga, L. Zhang, A.M. Viloria-Petit, A.A. Ogunjimi, M.R. Inanlou, E. Chiu, M. Buchanan, A.N. Hosein, M. Basik, J.L. Wrana, Exosomes mediate stromal mobilization of autocrine wnt-pcp signaling in breast cancer cell migration, Cell 151(7) (2012) 1542-1556.
20. D.D. Taylor, C. Gercel-Taylor, Exosomes/microvesicles: mediators of cancer-associated immunosuppressive microenvironments, Semin Immunopathol 33(5) (2011) 441-454.
21. K.B. Challagundla, P.M. Wise, P. Neviani, H. Chava, M. Murtadha, T. Xu, R. Kennedy, C. Ivan, X. Zhang, I. Vannini, F. Fanini, D. Amadori, G.A. Calin, M. Hadjidaniel, H. Shimada, A. Jong, R.C. Seeger, S.

Asgharzadeh, A. Goldkorn, M. Fabbri, Exosome-mediated transfer of micrornas within the tumor microenvironment and neuroblastoma resistance to chemotherapy, J Natl Cancer Inst 107(7) (2015).

22. Y.C. Au, N.N. Co, T. Tsuruga, T.L. Yeung, S.Y. Kwan, C.S. Leung, Y. Li, E.S. Lu, K. Kwan, K.K. Wong, R. Schmandt, K.H. Lu, S.C. Mok, Exosomal transfer of stroma-derived mir21 confers paclitaxel resistance in ovarian cancer cells through targeting apaf1, Nat Commun 7 (2016) 11150.
23. D.M. Epstein, Special delivery: microrna-200-containing extracellular vesicles provide metastatic message to distal tumor cells, J Clin Invest 124(12) (2014) 5107-5108.
24. A. Kozomara, M. Birgaoanu, S. Griffiths-Jones, Mirbase: from microrna sequences to function, Nucleic Acids Res 47(D1) (2019) D155-D162.
25. A.M. Mohr, J.L. Mott, Overview of microrna biology, Semin Liver Dis 35(1) (2015) 3-11.
26. X.G. Sun, X.C. Lin, J.X. Diao, Z.L. Yu, K. Li, Pi (spleen)-deficiency syndrome in tumor microenvironment is the pivotal pathogenesis of colorectal cancer immune escape, Chin J Integr Med 22(10) (2016) 789-794.
27. B. Wu, M.Y. Shen, H.P. Chen, Y.P. Liu, F. Wang, L. Chen, [spleen deficiency and phlegm dampness syndrome model in rats treated by citri reticulatae pericarpium based on metabolomics], Zhongguo Zhong Yao Za Zhi 47(15) (2022) 4136-4147.
28. Y. Wang, P. Li, S. Mao, Z. Mo, Z. Cao, J. Luo, M. Zhou, X. Liu, S. Zhang, L. Yu, Exosome ctla-4 regulates pten/cd44 signal pathway in spleen deficiency internal environment to promote invasion and metastasis of hepatocellular carcinoma, Front Pharmacol 12 (2021) 757194.
29. A. Nagy, A. Lanczky, O. Menyhart, B. Gyorffy, Author correction: validation of mirna prognostic power in hepatocellular carcinoma using expression data of independent datasets, Sci Rep 8(1) (2018) 11515.
30. M. Jarosz-Biej, R. Smolarczyk, T. Cichon, N. Kulach, Tumor microenvironment as a "game changer" in cancer radiotherapy, Int J Mol Sci 20(13) (2019).
31. I. Vitale, G. Manic, L.M. Coussens, G. Kroemer, L. Galluzzi, Macrophages and metabolism in the tumor microenvironment, Cell Metab 30(1) (2019) 36-50.
32. B. Arneth, Tumor microenvironment, Medicina (Kaunas) 56(1) (2019).
33. C. Chen, H. Chen, Y. Zhang, H.R. Thomas, M.H. Frank, Y. He, R. Xia, Tbtools: an integrative toolkit developed for interactive analyses of big biological data, Mol Plant 13(8) (2020) 1194-1202.
34. S.M. Arias-Mejias, K.Y. Warda, E. Quattrocchi, H. Alonso-Quinones, S. Sominidi-Damodaran, A. Meves, The role of integrins in melanoma: a review, Int J Dermatol 59(5) (2020) 525-534.
35. X. Shen, S. Wang, Q. Lu, Y. Guo, L. Qian, Translating cancer exosomes detection into the color change of phenol red based on target-responsive dna microcapsules, Anal Chim Acta 1192 (2022) 339357.
36. R. Kalluri, The biology and function of exosomes in cancer, J Clin Invest 126(4) (2016) 1208-1215.
37. C. Li, A.F. Teixeira, H.J. Zhu, D.P. Ten, Cancer associated-fibroblast-derived exosomes in cancer progression, Mol Cancer 20(1) (2021) 154.

38. I. Kaymak, K.S. Williams, J.R. Cantor, R.G. Jones, Immunometabolic interplay in the tumor microenvironment, Cancer Cell 39(1) (2021) 28-37.
39. O. Meurette, P. Mehlen, Notch signaling in the tumor microenvironment, Cancer Cell 34(4) (2018) 536-548.
40. A. Wong-Rolle, H.K. Wei, C. Zhao, C. Jin, Unexpected guests in the tumor microenvironment: microbiome in cancer, Protein Cell 12(5) (2021) 426-435.
41. A.E. Denton, E.W. Roberts, D.T. Fearon, Stromal cells in the tumor microenvironment, Adv Exp Med Biol 1060 (2018) 99-114.
42. Y. Oya, Y. Hayakawa, K. Koike, Tumor microenvironment in gastric cancers, Cancer Sci 111(8) (2020) 2696-2707.
43. R.J. Deberardinis, Tumor microenvironment, metabolism, and immunotherapy, N Engl J Med 382(9) (2020) 869-871.
44. T. Yang, K.Y. Sim, G.H. Ko, J.S. Ahn, H.J. Kim, S.G. Park, Fam167a is a key molecule to induce bcr-abl-independent tki resistance in cml via noncanonical nf-kappab signaling activation, J Exp Clin Cancer Res 41(1) (2022) 82.
45. A. Hoshino, B. Costa-Silva, T.L. Shen, G. Rodrigues, A. Hashimoto, M.M. Tesic, H. Molina, S. Kohsaka, A. Di Giannatale, S. Ceder, S. Singh, C. Williams, N. Soplop, K. Uryu, L. Pharmer, T. King, L. Bojmar, A.E. Davies, Y. Ararso, T. Zhang, H. Zhang, J. Hernandez, J.M. Weiss, V.D. Dumont-Cole, K. Kramer, L.H. Wexler, A. Narendran, G.K. Schwartz, J.H. Healey, P. Sandstrom, K.J. Labori, E.H. Kure, P.M. Grandgenett, M.A. Hollingsworth, M. de Sousa, S. Kaur, M. Jain, K. Mallya, S.K. Batra, W.R. Jarnagin, M.S. Brady, O. Fodstad, V. Muller, K. Pantel, A.J. Minn, M.J. Bissell, B.A. Garcia, Y. Kang, V.K. Rajasekhar, C.M. Ghajar, I. Matei, H. Peinado, J. Bromberg, D. Lyden, Tumour exosome integrins determine organotropic metastasis, Nature 527(7578) (2015) 329-335.
46. I. Wortzel, S. Dror, C.M. Kenific, D. Lyden, Exosome-mediated metastasis: communication from a distance, Dev Cell 49(3) (2019) 347-360.
47. H. Zhang, L. Wang, C. Li, Y. Yu, Y. Yi, J. Wang, D. Chen, Exosome-induced regulation in inflammatory bowel disease, Front Immunol 10 (2019) 1464.
48. D. Hanahan, Hallmarks of cancer: new dimensions, Cancer Discov 12(1) (2022) 31-46.
49. M.C. Juan-Rivera, M. Martinez-Ferrer, Integrin inhibitors in prostate cancer, Cancers (Basel) 10(2) (2018).
50. J. Niu, Z. Li, The roles of integrin alphavbeta6 in cancer, Cancer Lett 403 (2017) 128-137.
51. A.A. Albittar, O. Alhalabi, O.I. Glitza, Immunotherapy for melanoma, Adv Exp Med Biol 1244 (2020) 51-68.
52. L.M. Cuevas, A.I. Daud, Immunotherapy for melanoma, Semin Cutan Med Surg 37(2) (2018) 127-131.
53. S.M. Ansell, F. Caligaris-Cappio, D.G. Maloney, Immunotherapy in lymphoma, Hematol Oncol 35 Suppl 1 (2017) 88-91.

54. R. Surana, S. Pant, Immunotherapy in gastrointestinal malignancies, Adv Exp Med Biol 1342 (2021) 259-272.
55. M. Frelaut, B. Besse, [immunotherapy in oncology], Rev Prat 71(10) (2021) 1051-1056.
56. K. Fukuda, Y. Saikawa, H. Yagi, N. Wada, T. Takahashi, Y. Kitagawa, Role of integrin alpha1 subunits in gastric cancer patients with peritoneal dissemination, Mol Med Rep 5(2) (2012) 336-340.
57. L. Peng, G. Jin, L. Wang, J. Guo, L. Meng, C. Shou, Identification of integrin alpha1 as an interacting protein of protein tyrosine phosphatase prl-3, Biochem Biophys Res Commun 342(1) (2006) 179-183.
58. L. Shang, X. Ye, G. Zhu, H. Su, Z. Su, B. Chen, K. Xiao, L. Li, M. Peng, T. Peng, Prognostic value of integrin variants and expression in post-operative patients with hbv-related hepatocellular carcinoma, Oncotarget 8(44) (2017) 76816-76831.

Figures

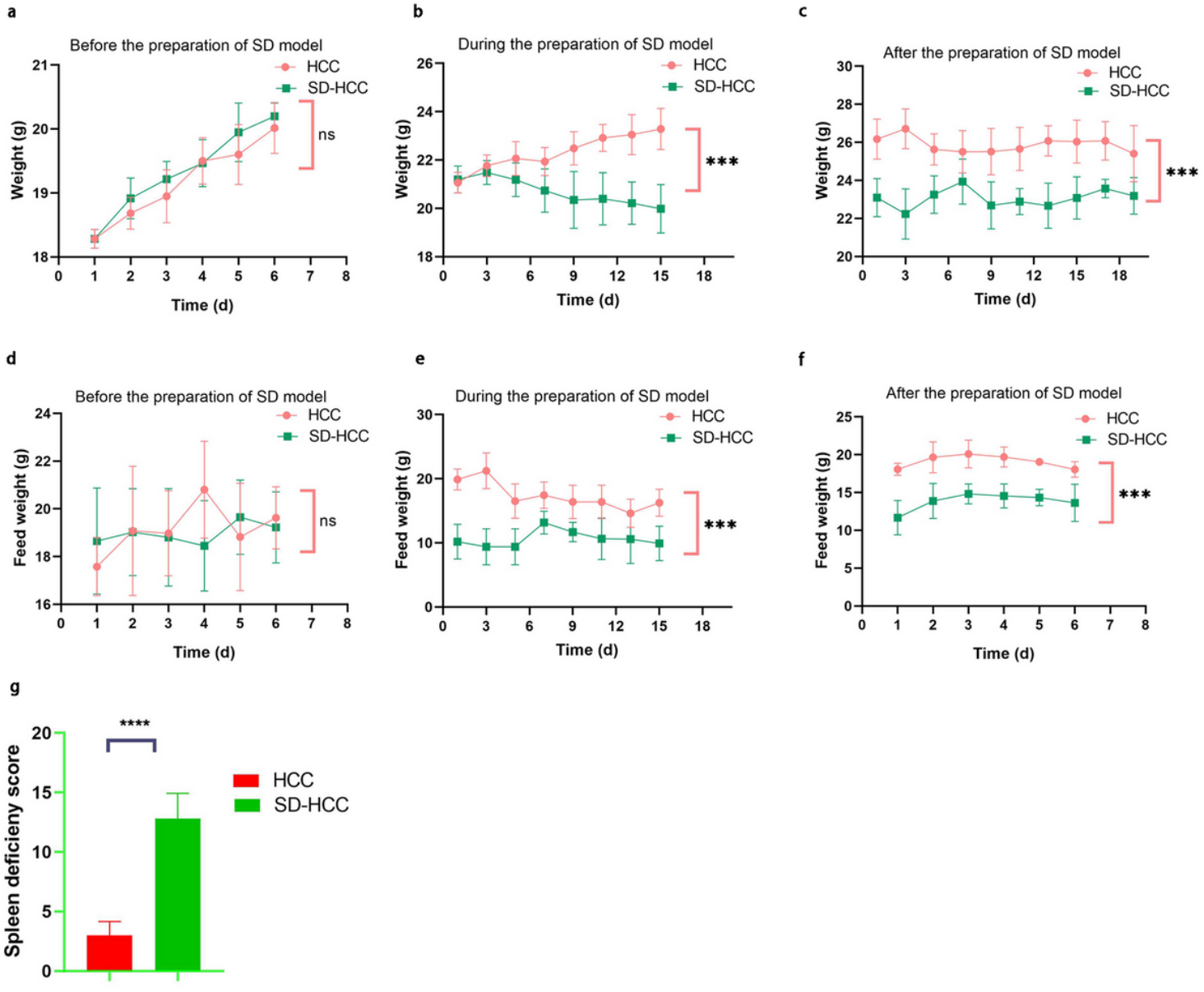

Figure 1

Differences before and after orthotopic liver transplantation in mice with spleen deficiency. **(a)** Statistical chart of body weight differences between the two mouse groups before modeling. **(b)** Statistical chart of body weight difference between the two groups during modeling. **(c)** Statistical chart of body weight difference between the two groups after modeling. **(d)** Differences in daily diet weight between the two groups before modeling. **(e)** Differences in daily diet weight between the two groups during modeling. **(f)** Differences in daily diet weight between the two groups after modeling. **(g)** The scores of spleen deficiency were different between the two groups of mice. *$p < 0.05$, **$p < 0.01$, ***$p < 0.001$, ****$p < 0.0001$.

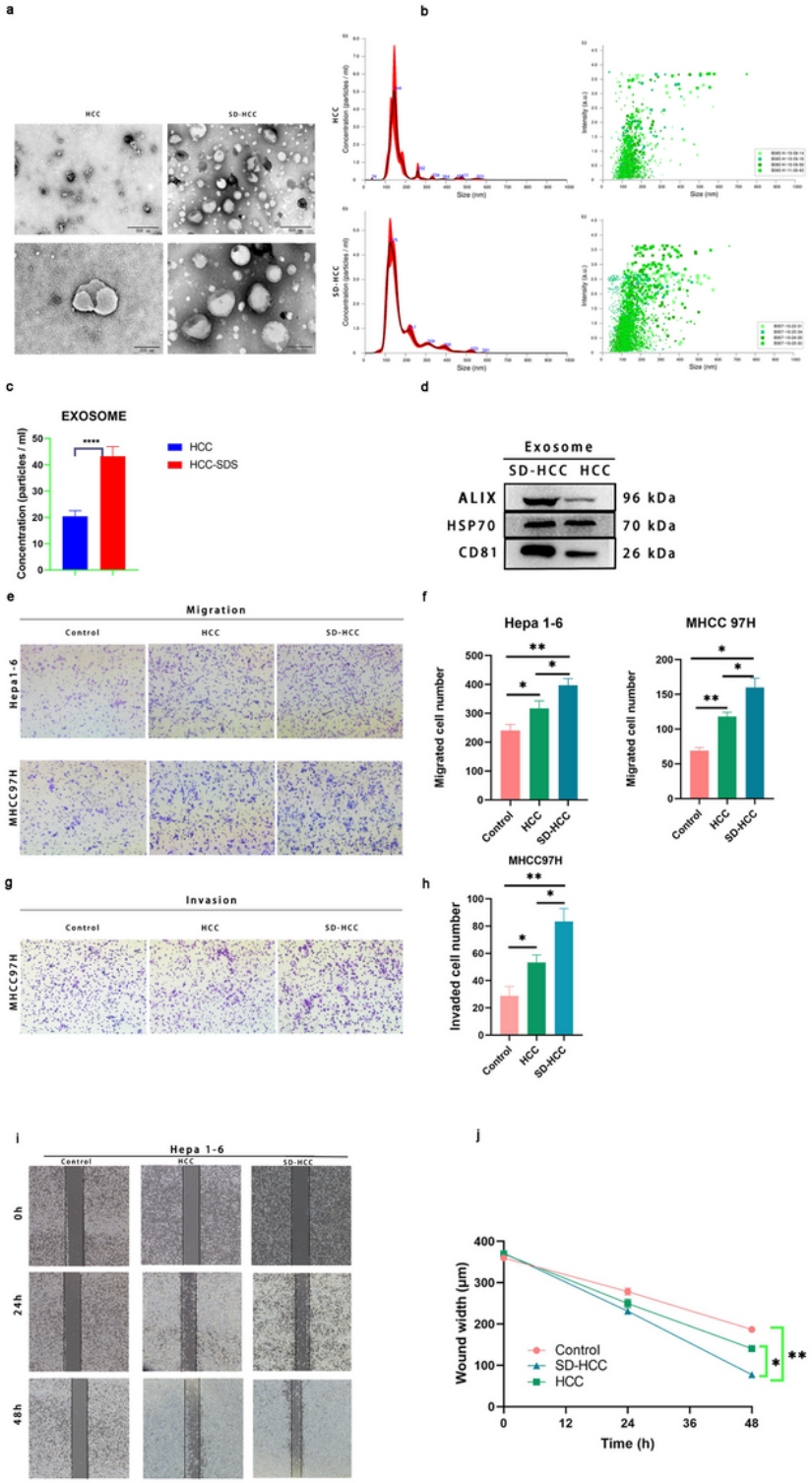

Figure 2

In vitro identification of and differences between exosomes from two mouse sources. **(a)** Electron microscopy images of exosomes from the plasma of different C57 mice (HCC and SD-HCC). Scale bars = 200 nm and 500 nm. **(b)** Nanoparticle tracking assay detection of exosomes in plasma from HCC and SD-HCC mice. **(c)** Statistical chart of the exosome concentration in the two groups. **(d)** Western blot analysis of surface markers (ALIX, HSP70, CD81) of exosomes from two groups of mice (samples are a

mixture of exosomes from 4 mice in each group). **(e)** Effects of exosomes from different mouse sources and of the blank (BLK) control on the migration ability of HCC cells. **(f)** Statistical chart of the cell migration abilities for the three groups. **(g)** Effects of exosomes from different mouse sources and of the blank (BLK) control on the invasion ability of HCC cells. **(h)** Statistical chart of the cell invasion abilities for the three groups. **(i)** Results of the cell scratch experiment for the Control, HCC exosome, and SD-HCC exosome groups. **(j)** Statistical chart of the cell scratch experimental results. *p< 0.05, **p < 0.01, ***p < 0.001, ****p < 0.0001. HCC, mice with hepatocellular carcinoma only; SD-HCC, mice with both spleen deficiency and hepatocellular carcinoma.

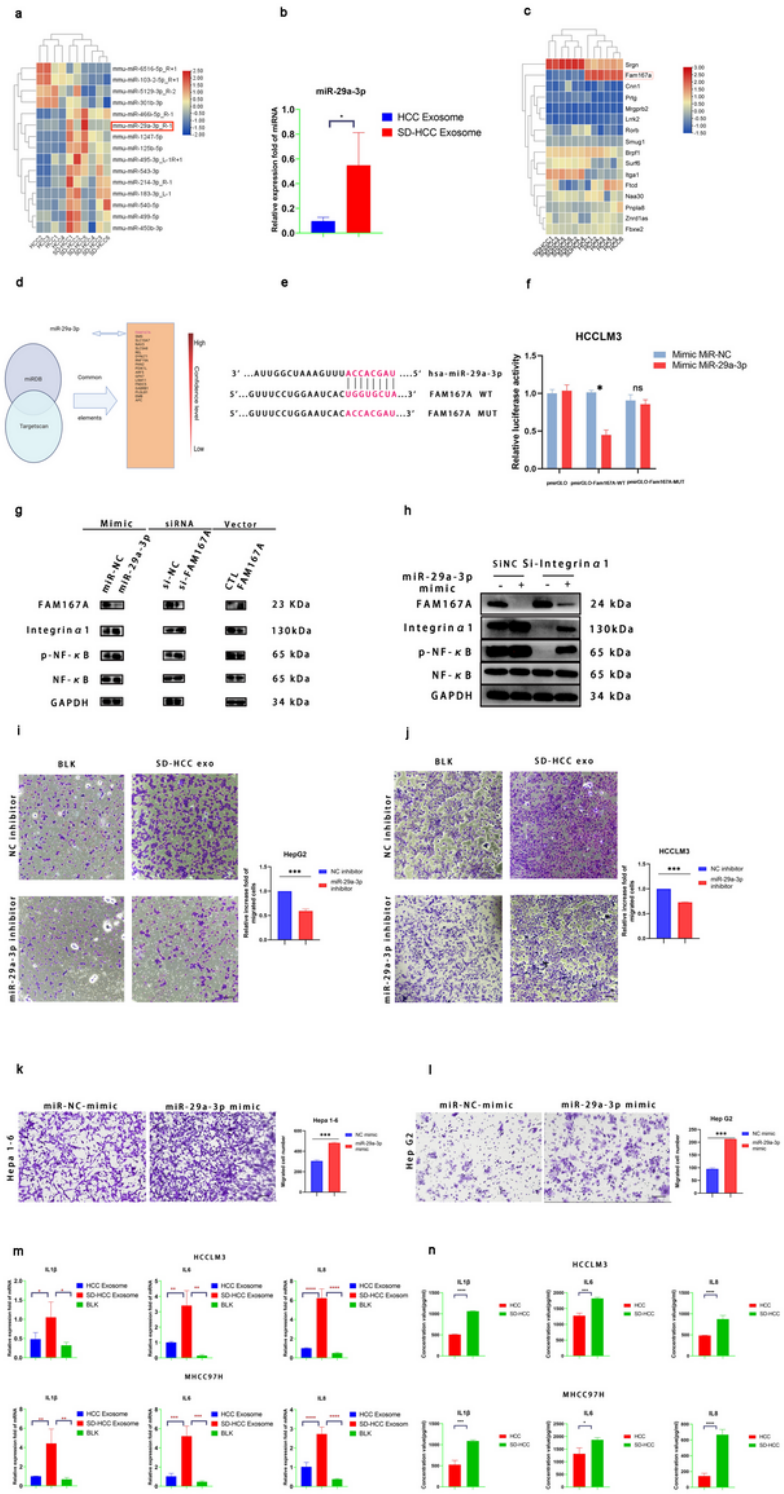

Figure 3

Exosomal miR-29a-3p regulated FAM167A–α1-integrin to activate the NF-κB pathway and promote inflammatory factor release. **(a)** The two groups of exosomes were sequenced to identify differentially expressed miRNAs. **(b)** qRT-PCR analysis of miRNA29a-3p expression differences between the two groups. **(c)** The differentially expressed gene *FAM167A*was obtained by RNA sequencing of hepatocellular carcinoma tissues from SD-HCC and HCC C57 mice. **(d)** Target gene prediction for miR-

29a-3p using two bioinformatics tools. **(e)** Wild-type and mutated type of binding sites between miR-29a-3p and FAM167A. **(f)** Relative luciferase activity in HCCLM3 cells subjected to the indicated treatments. **(g)** Immunoblots of the indicated proteins in HCCLM3 cells subjected to the indicated treatments. **(h)** Effect of miR-29a-3p on the expression of the indicated proteins in HCCLM3 cells with or without the suppression of α1-integrin expression. **(i, j)** Comparison of the migration abilities of HepG2 and HCCLM3 cells treated with exosomes derived from SD-HCC C57 mice stably expressing the miR-29a-3p inhibitor or negative control. Migrated cells were counted, and representative images are shown. Scale bar = 150 μm. **(k, l)** Effect of the miR-29a-3p mimic on the migration abilities of Hepa1-6 and HepG2 cells. Scale bar = 150 μm. **(m)** qRT-PCR analysis of the expression of interleukin genes in MHCC97H and HCCLM3 cells treated with exosomes extracted from different C57 mouse plasmas or the blank control. **(n)** ELISA analysis of the differences in interleukin levels after co-incubation of hepatoma cells with different exosomes. *p< 0.05, **p < 0.01, ***p < 0.001, ****p < 0.0001. HCC, mice with hepatocellular carcinoma only; SD-HCC, mice with both spleen deficiency and hepatocellular carcinoma; ELISA, enzyme-linked immunosorbent assay; qRT-PCR, real-time reverse transcription-polymerase chain reaction.

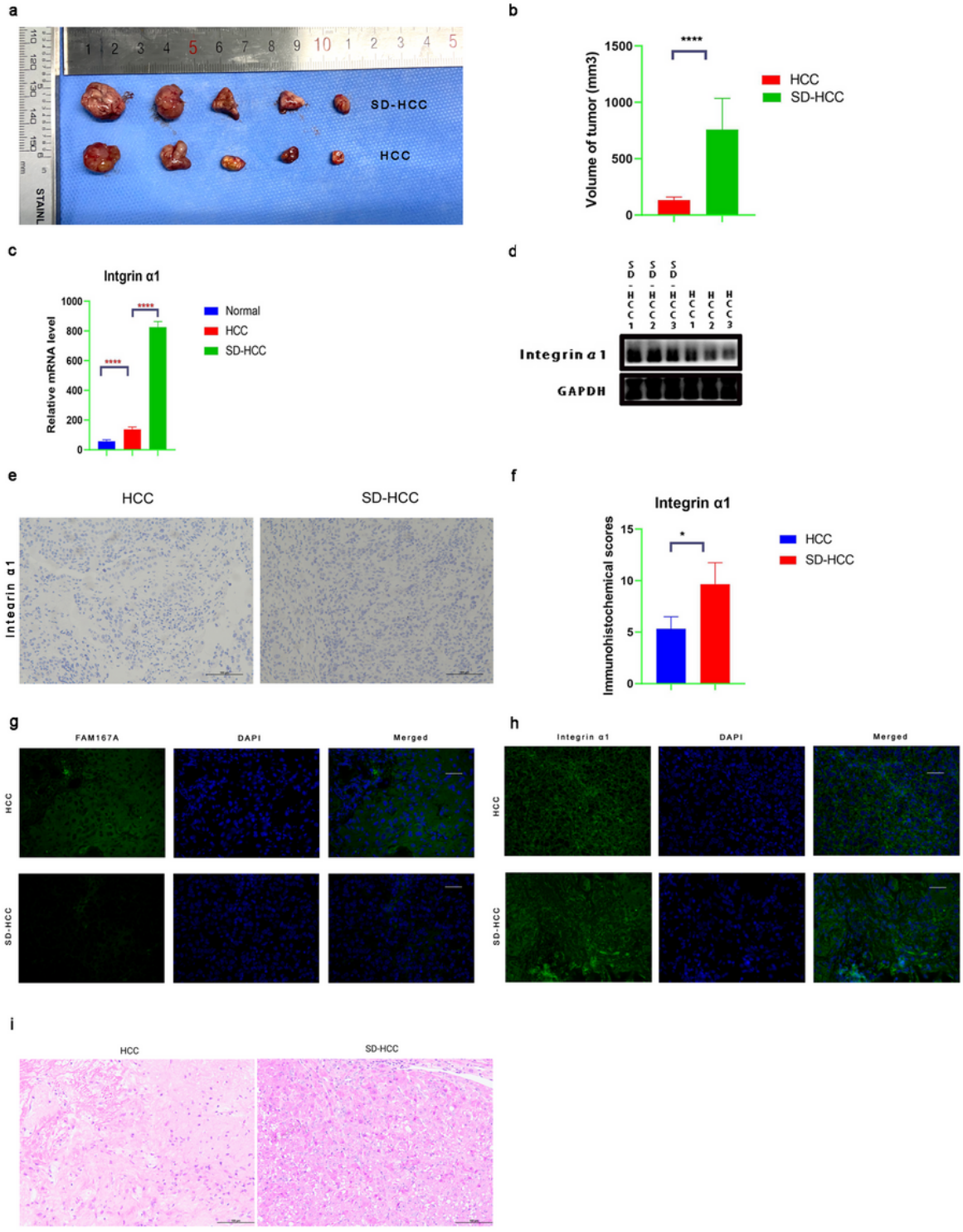

Figure 4

Spleen deficiency changed the tumor immune microenvironment and promoted tumor growth in vivo. **(a)** Differences in tumor size between the two groups of mice. **(b)** Statistical chart of the difference in tumor sizes between the two groups of mice. **(c)** qRT-PCR analysis of the changes in α1-integrin expression level in the liver tissue of the two groups of mice and normal mice. **(d)** Western blot of the changes in protein levels in hepatocellular carcinoma tissues from the two groups of mice. **(e)** Immunohistochemical

detection of the difference in α1-integrin levels between tumor tissues from the two groups of mice. **(f)** Statistical chart of the immunohistochemical results. **(g)** Immunofluorescence staining to detect the difference in *FAM167A* gene expression in liver cancer tissues between the two groups of mice. Scale bar = 100 μm. **(h)** Immunofluorescence staining to detect the difference in α1-integrin gene expression in liver cancer tissues between the two groups of mice. Scale bar = 100 μm. **(i)** HE staining of the tumors from the two mouse groups. Data are presented as the means ± SD. Student's *t*-test was used to analyze the data. *$p < 0.05$, **$p < 0.01$, ***$p < 0.001$, ****$p < 0.0001$.

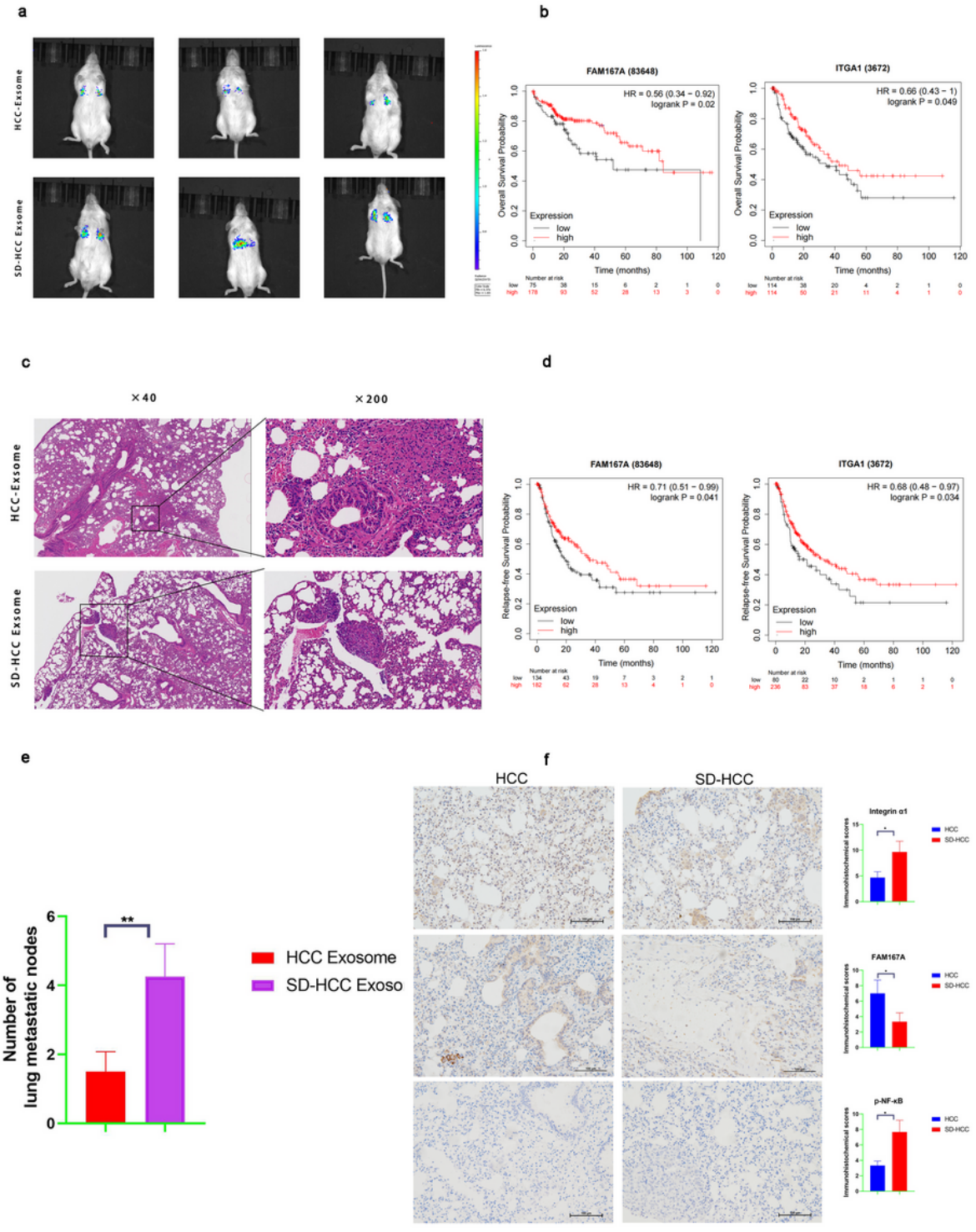

Figure 5

Effects of two groups of exosomes on lung metastasis in immunodeficient mice. **(a)** Representative images of lung metastases in immunodeficient mice treated with exosomes derived from two different sets of mouse plasma, as determined by luciferase-based bioluminescence imaging. **(b)** Kaplan–Meier curves of overall survival (OS) for patients with low versus high expression of α1-integrin and FAM167A in the GEO and TCGA databases. **(c)** HE staining of metastatic lung nodules in two groups of mice. **(d)** Kaplan–Meier curves of recurrence/relapse-free survival (RFS) for patients with low versus high expression of α1-integrin and FAM167A in the GEO and TCGA databases. **(e)** Statistical chart of the number of metastatic lung nodules. **(f)** Immunohistochemical analysis of the differences in metastatic lung nodules between the two groups. *$p < 0.05$, **$p < 0.01$, ***$p < 0.001$, ****$p < 0.0001$.

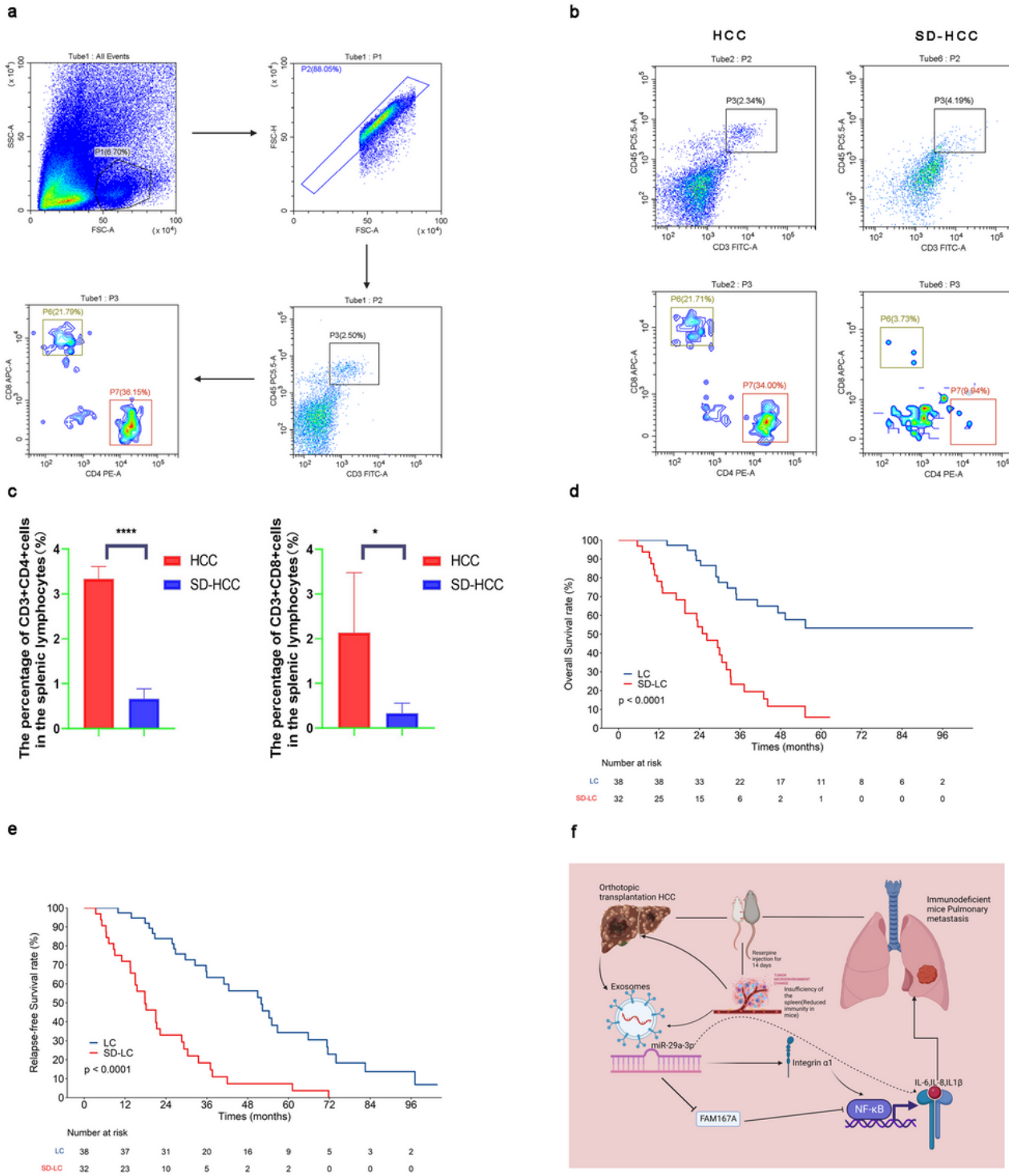

Figure 6

Spleen deficiency changes the immune status of mice and affects the overall survival of liver cancer patients. **(a)** Flow cytometry gating strategy for detecting tumor-infiltrating leukocytes. **(b)** Flow cytometric quantification showing the decreased infiltration of $CD3^+CD4^+$ and $CD3^+CD8^+$ T cells. **(c)** Statistical chart of the percentages of $CD3^+CD4^+$ and $CD3^+CD8^+$ T cells in the splenic lymphocytes (%). **(d)** Differences in overall survival rate between liver cancer patients with spleen deficiency symptoms

(SD-LC) and those without spleen deficiency symptoms (LC). **(e)** Difference in relapse-free survival rates between patients in the SD-HCC group and those in the HCC group. *p < 0.05, **p < 0.01, ***p < 0.001, ****p < 0.0001. **(f)** Schematic illustration of the pathway through which exosomal miR-29a-3p promotes lung metastasis from liver cancer under spleen deficiency conditions.

Supplementary Files

This is a list of supplementary files associated with this preprint. Click to download.

- TableS1primerdesign.xlsx
- TableS2.siRNAprimersequencesforplasmidconstruction.xlsx
- WBOriginalmaterial.pdf